particles

IMPACT FACTOR 1.4

CITESCORE 0.4

Article

Hyperonic Interactions in Neutron Stars

Semyon Mikheev, Dmitry Lanskoy, Artur Nasakin and Tatiana Tretyakova

Special Issue

Infinite and Finite Nuclear Matter (INFINUM)

Edited by

Dr. Evgeni Kolomeitsev, Dr. Nikolai Antonenko, Prof. Dr. David Blaschke, Prof. Dr. Victor Braguta and Dr. Isaac Vidaña

MDPI

https://doi.org/10.3390/particles6030054

particles

MDPI

Article

Hyperonic Interactions in Neutron Stars

Semyon Mikheev [1,2,*], Dmitry Lanskoy [1], Artur Nasakin [1] and Tatiana Tretyakova [1,2]

[1] Faculty of Physics, Lomonosov Moscow State University, Leninskie Gory, Moscow 119991, Russia; lanskoy@sinp.msu.ru (D.L.); nasakin.ai18@physics.msu.ru (A.N.); tretyakova@srd.sinp.msu.ru (T.T.)
[2] Skobeltsyn Institute of Nuclear Physics, Lomonosov Moscow State University (SINP MSU), Leninskie Gory, Moscow 119991, Russia
* Correspondence: mikheev.sa16@physics.msu.ru

Abstract: The matter of neutron stars is characterised by the density of the order of typical nuclear densities; hence, it can be described with methods of nuclear physics. However, at high densities, some effects that are absent in nuclear and hypernuclear physics can appear, and this makes neutron stars a good place for studying the properties of baryonic interactions. In the present work, we consider neutron stars consisting of nucleons, leptons and Λ hyperons with Skyrme baryonic forces. We study the character of the ΛN interactions taking place in neutron stars at high densities. In particular, we show the difference between three-body ΛNN and density-dependent ΛN forces. We also demonstrate that the Skyrme ΛN forces proportional to nuclear density are better suited for the modelling of neutron stars than the forces proportional to fractional powers of density. Finally, we emphasize the importance of the point of appearance of hyperons in a further search for parameterizations which are suitable for describing neutron stars.

Keywords: neutron stars; hyperons; baryonic interaction; nuclear matter

check for updates

Citation: Mikheev, S.; Lanskoy, D.; Nasakin, A.; Tretyakova, T. Hyperonic Interactions in Neutron Stars. *Particles* **2023**, *6*, 847–863. https://doi.org/10.3390/particles6030054

Academic Editors: Evgeni Kolomeitsev, Nikolai Antonenko, David Blaschke, Victor Braguta, Isaac Vidaña and Armen Sedrakian

Received: 29 June 2023
Revised: 7 August 2023
Accepted: 22 August 2023
Published: 8 September 2023

Copyright: © 2023 by the authors. Licensee MDPI, Basel, Switzerland. This article is an open access article distributed under the terms and conditions of the Creative Commons Attribution (CC BY) license (https://creativecommons.org/licenses/by/4.0/).

1. Introduction

Neutron stars are stars in hydrostatic equilibrium that consist mostly of neutrons and have the density of the order of typical nuclear densities. Currently, neutron stars are observed in all parts of the electromagnetic spectrum. The vast majority of measurements of neutron star masses were conducted using radio observations of rotating pulsars in binary systems. At present, more than 2500 pulsars are known in the galaxy, but about 90% of them are isolated, and their masses cannot be measured using current methods. Among the neutron stars with masses measured reliably, the majority fall into the range of 1.3 to 1.5 $M_\odot$ [1,2]. However, there are neutron stars with masses about 2 $M_\odot$. The most massive of these are currently the pulsars PSR J1614-2230 [3,4], PSR J0348+0432 [5] and PSR J0740+6620 [6,7] with masses of $(1.908 \pm 0.016)\ M_\odot$, $(2.01 \pm 0.04)\ M_\odot$ and $(2.08 \pm 0.07)\ M_\odot$, respectively, at 68.3% credibility. Additionally, PSR J0952-0607 [8] with a mass of $(2.35 \pm 0.17)\ M_\odot$ was observed recently, and it is currently the fastest known spinning neutron star in the galaxy. Thus, the latest observational data indicate that the maximum mass of 2 $M_\odot$ should be reached in theoretical models. The construction of such models appears to be a difficult task due to the reduction in the maximum mass in models with hyperons. This problem will be discussed below in more detail.

Another measured characteristic of neutron stars is their radii. The majority of methods for their measurement are based on the analysis of thermal radiation from the surface of the star. Such measurements require detailed theoretical modelling of this radiation and careful selection of its sources, considering that the surface radiation of a star can be distorted due to the accretion of matter from the companion star or from a strong magnetic field. Therefore, it is difficult to measure the radii of neutron stars in binary systems, and it is rarely possible to simultaneously measure both the mass and the radius of a neutron star. However, relatively accurate radius values were obtained, for instance, for pulsar PSR

J0740+6620 (which was mentioned above) by two independent groups: $12.39^{+1.30}_{-0.98}$ km (68 % credible interval) in [9] and $13.7^{+2.6}_{-1.5}$ in [10]. Later, these results were revised in [11], where the value of $12.97^{+1.56}_{-1.39}$ km was reported (68% credible interval).

A wide range of extreme states of matter that cannot be studied in terrestrial conditions are realized in neutron stars, making them a source of information on the properties of baryonic interactions and nuclear matter. Additional sensitivity to certain properties of baryonic interactions can arise in these states; thus, the study of neutron stars is of great importance for nuclear physics. Alternatively, the development of the theory of many-body nuclear systems is required for a better understanding of neutron star physics. In the present work, we do not pretend to conduct a comprehensive description of the observed data; rather, we study the influence of certain properties of hyperonic interactions on the characteristics of neutron stars.

At densities that are close to the normal nuclear density, the matter of neutron stars presumably consists of neutrons, protons, electrons and muons. At densities that are several times higher, hyperons may also appear. As the density increases, Λ-hyperons are expected to appear first; thus, in the present work, we consider neutron stars to consist of nucleons, leptons and Λ-hyperons. Although the appearance of hyperons in neutron star matter seems to be the most likely option today, it also is the cause of the problem known as the "hyperon puzzle". In particular, the models incorporating hyperons predict maximum masses smaller than the masses in models without hyperons, and also smaller than the masses obtained from observations. This phenomenon arises due to the fact that the presence of hyperons considerably softens the equations of state of neutron star matter. To stand up to this challenge, a deeper study of the hyperon–nucleon and hyperon–hyperon interactions, as well as a search for more stiff equations of state, are required [12,13].

Various attempts to resolve the hyperon puzzle have been reported in the literature (for a recent brief review, see [14]). In [15], the so-called universal three-baryon interaction was shown to potentially resolve the puzzle. An important role of the three-baryon interactions was discussed later in [13,16–18]. More exotic explanations like deconfined quark matter in the central region or in the whole star (see [13,14]), as well as dark matter particles in neutron stars [19], have also been proposed.

Since the pioneering paper of [20], the relativistic mean field theory in its various versions has become one of the most frequently used approaches in this field. After [20], our knowledge of hypernuclear properties was enhanced substantially; thus, the parameters of the corresponding relativistic energy density functional are constrained more strictly. However, it is yet possible to come up with many sets of parameters that are compatible with hypernuclear data. Additional theoretical refinements were suggested in the last few decades, e.g., nonlinearities in the scalar and vector fields, the addition of the hidden-strangeness scalar and vector fields, the density dependence of the coupling constants, etc. The current progress in this approach has been reviewed recently [21]. Within the relativistic mean field theory, various attempts to solve the hyperon puzzle are known, e.g., refs. [22–32]. Essentially, a sufficient repulsion at short baryon–baryon distances due to usual and/or hidden strangeness vector fields is introduced to resolve the puzzle.

However, there is no commonly accepted solution thus far. The main reason for this is that the properties of the baryonic interactions occurring at high densities that play a crucial role in this problem have been studied insufficiently; thus, it is difficult to independently check any of the explanations of the hyperon puzzle.

To describe the baryonic matter of neutron stars, we used an approach based on the Skyrme interaction, which is a self-consistent non-relativistic mean field model that was developed for nuclear systems. Skyrme potential parameterizations include a large set of parameters that are obtained from the empirical data of atomic nuclei and hypernuclei, which allow for the description of nucleon–nucleon, nucleon–hyperon and hyperon–hyperon interactions in a single approach. There is a wide variety of Skyrme potential parametrizations that describe the matter equally well at nuclear densities, but these same parametrizations can lead to completely different results at higher densities.

The Skyrme model was widely used in various works in order to study the properties of nuclei and nuclear matter [18]. It was applied to the description of neutron stars [33,34], including those with Λ-hyperons, where the authors attempted to solve the hyperon puzzle [35] and explore different properties of baryonic interactions [36]. In this work, we focus on examining the properties of the ΛN interactions which have been studied relatively well for hypernuclei. By construction, the Skyrme interaction contains three-body forces or density-dependent, repulsive two-body forces.

It is worth noting that the Skyrme model is non-relativistic, which leads to limitations in the high-density region, but its flexibility and a large number of different parameterizations make it a good choice for realizing the goals of this work.

Renewed interest in neutron stars physics was induced by one of the most important discoveries in this area. On 17 August 2017, gravitational waves from a neutron star merger were registered for the first time by the detector system LIGO-Virgo (GW170817) [37]. Information about electromagnetic and gravitational waves can be used, in particular, to obtain restrictions on the equation of state of dense nuclear matter. Nowadays, neutron star mergers are considered to be an important factor in the nucleosynthesis of heavy elements in the universe. In 2019, the first astrophysical confirmation of such process was obtained when the spectrum of strontium was identified in the data from GW170817 [38]. Moreover, it became the first experimental evidence that the matter of neutron stars is indeed neutron-rich. Among other things, the registration of GW170817 provided us with the first experimental estimates of such a characteristic, the tidal deformability of a neutron star.

Later, the GW190425 event [39] was observed, but its assignment as the neutron star merger remains ambiguous.

Tidal deformability shows how the shape of a star changes under the influence of external gravitational forces. In the present work, following the majority of works on tidal deformability, we consider only quadrupole deformations. Tidal deformability coefficient λ is defined as the ratio of the quadrupole moment of the star Q_{ij} to the external tidal field ε_{ij} [40,41]:

$$Q_{ij} = -\lambda \varepsilon_{ij}. \tag{1}$$

We use a dimensionless tidal deformability coefficient:

$$\Lambda = \frac{\lambda}{M^5}, \tag{2}$$

where M is the mass of the neutron star. The tidal deformability coefficient provides us with an additional instrument for the selection of equations of state and parameters of interactions.

2. Methods

2.1. Skyrme Potential

We use the nucleon–nucleon [42]

$$\begin{aligned} V_{NN}(\mathbf{r_1}, \mathbf{r_2}) = {} & t_0(1 + x_0 P_\sigma)\delta(\mathbf{r_1} - \mathbf{r_2}) \\ & + \frac{1}{2} t_1(1 + x_1 P_\sigma)[\mathbf{P'}^2 \delta(\mathbf{r_1} - \mathbf{r_2}) + \delta(\mathbf{r_1} - \mathbf{r_2})\mathbf{P}^2] \\ & + t_2(1 + x_2 P_\sigma)\mathbf{P'}\delta(\mathbf{r_1} - \mathbf{r_2})\mathbf{P} \\ & + iW_0 \boldsymbol{\sigma}[\mathbf{P'} \times \delta(\mathbf{r_1} - \mathbf{r_2})\mathbf{P}] \end{aligned} \tag{3}$$

and the hyperon–nucleon [43]

$$\begin{aligned} V_{\Lambda N}(\mathbf{r_\Lambda}, \mathbf{r_N}) &= u_0(1+\xi_0 P_\sigma)\delta(\mathbf{r_\Lambda}-\mathbf{r_N}) \\ &+ \frac{1}{2}u_1[\mathbf{P'}^2\delta(\mathbf{r_\Lambda}-\mathbf{r_N}) + \delta(\mathbf{r_\Lambda}-\mathbf{r_N})\mathbf{P}^2] \\ &+ u_2\mathbf{P'}\delta(\mathbf{r_\Lambda}-\mathbf{r_N})\mathbf{P} \\ &+ iW_0^\Lambda\mathbf{P'}\delta(\mathbf{r_\Lambda}-\mathbf{r_N})[\boldsymbol{\sigma}\times\mathbf{P}] \end{aligned} \tag{4}$$

Skyrme potentials in the standard form. In (3) and (4), $\mathbf{P} = (2i)^{-1}(\nabla_1 - \nabla_2)$ is the operator of the relative momentum acting on the ket while $\mathbf{P'}$ acts on the bra, $P_\sigma = \frac{1}{2}(1+\boldsymbol{\sigma_1}\boldsymbol{\sigma_2})$ is the spin exchange operator and $\boldsymbol{\sigma_i}$ are the Pauli spin matrices. For the ΛN interaction, the 1 and 2 indices should be replaced by Λ and N.

The two-body interaction V_{NN} depends on the parameters $t_i, x_i (i = 0, 1, 2)$ and W_0. Parameters t_0 and t_1 correspond to the terms acting on relative even states (in fact, only s-states), and t_2 governs the term acting in relative odd states (p-states). Using the x_i parameters allows one to influence the proton–neutron asymmetry properties. Parameter W_0 determines the one-body spin–orbit strength. Numerous parametrizations of nucleon–nucleon forces have been obtained by fitting certain characteristics of atomic nuclei and nuclear matter. Parameters $u_i, (i = 0, 1, 2)$, ξ_0 and W_0^Λ of the two-body hyperon–nucleon interaction $V_{\Lambda N}$ are introduced in a similar way; their values are also obtained mainly by fitting the experimental spectra of the hypernuclei. The spin–orbit terms in (3) and (4) vanish in uniform non-polarized nuclear matter and will not be considered further.

Reliable (and scarce) information on the $\Lambda\Lambda$ interaction has been obtained from the data on $\Lambda\Lambda$ hypernuclei [44]. Since the $\Lambda\Lambda$ hypernuclei were so far observed only in the ground states with both hyperons in the 1s state, there is no information on the p-wave $\Lambda\Lambda$ interaction. Thus, we use the simplified $\Lambda\Lambda$ Skyrme potential from [45].

$$\begin{aligned} V_{\Lambda\Lambda}(\mathbf{r_1}, \mathbf{r_2}) &= \lambda_0\delta(\mathbf{r_1}-\mathbf{r_2}) \\ &+ \frac{1}{2}\lambda_1[\mathbf{P'}^2\delta(\mathbf{r_1}-\mathbf{r_2}) + \delta(\mathbf{r_1}-\mathbf{r_2})\mathbf{P}^2]. \end{aligned} \tag{5}$$

Many-body effects other than (3) and (4) should also be included. For nucleonic interaction, they may be represented as the three-body NNN force:

$$V_{123}(\mathbf{r_1}, \mathbf{r_2}, \mathbf{r_3}) = t_3\delta(\mathbf{r_1}-\mathbf{r_2})\delta(\mathbf{r_2}-\mathbf{r_3}) \tag{6}$$

or the density-dependent NN force:

$$V_{12}(\mathbf{r_1}, \mathbf{r_2}, n) = \frac{1}{6}t_3(1+x_3P_\sigma)\delta(\mathbf{r_1}-\mathbf{r_2})n^\alpha(\frac{\mathbf{r_1}+\mathbf{r_2}}{2}), \tag{7}$$

where n is the nucleon density. Forces (6) and (7) lead to equivalent results in matter at $x_3 = 1$ and $\alpha = 1$ [42].

Similarly, for hyperonic interactions the three-body ΛNN force

$$V_{\Lambda NN}(\mathbf{r_\Lambda}, \mathbf{r_{N1}}, \mathbf{r_{N2}}) = u_3\delta(\mathbf{r_\Lambda}-\mathbf{r_{N1}})\delta(\mathbf{r_\Lambda}-\mathbf{r_{N2}}) \tag{8}$$

or density-dependent ΛN force

$$V_{\Lambda N}(\mathbf{r_\Lambda}, \mathbf{r_N}, n) = \frac{3}{8}u_3(1+\xi_3P_\sigma)\delta(\mathbf{r_\Lambda}-\mathbf{r_N})n^\gamma(\frac{\mathbf{r_\Lambda}+\mathbf{r_N}}{2}) \tag{9}$$

are introduced [43,46].

At $\gamma = 1$ and $\xi_3 = 0$, (8) and (9) are almost equivalent for Λ hypernuclei and exactly equivalent for symmetric (with equal numbers of protons and neutrons) nuclear matter. The issue of equivalence is discussed in more detail in [47]. However, neutron stars are

neutron-rich nuclear systems, and said equivalence is violated. Moreover, the force (9) at $\gamma \neq 1$ apparently is not equivalent to (8). We study how different hyperonic many-body forces manifest in neutron stars.

2.2. Neutron Star Matter and Tidal Deformability

We consider the chemically equilibrated matter consisting of nucleons, leptons and Λ-hyperons. Usual conditions of the chemical equilibrium in terms of chemical potentials are used (see, e.g., ref. [20]). Using Skyrme potentials (3)–(9), we calculate in the standard way the energy density, pressure and chemical potentials, and determine the particle fractions $Y_i (i = p, n, \Lambda, \mu, e)$ from the equilibrium conditions. Repeating these calculations at various densities, we obtain the equation of state of the neutron star matter.

With the equation of state, we are in position to solve the Tolman–Oppenheimer–Volkov equation [48,49] at various central densities, which gives the $M(R)$ dependence and, particularly, the maximum mass of the neutron star. We follow the methodology used in [34,36] in the equation of state and $M(R)$ calculations. We also employ the equation of state of the neutron star crust using approximations obtained in [50].

Tidal deformability is represented [51] in terms of the Love tidal number k_2 and compactness parameter $C \equiv M/R$

$$\Lambda = \frac{2}{3} k_2 C^{-5}, \tag{10}$$

while k_2 is derived from the following expression [52–54]:

$$\begin{aligned} k_2 = {} & \frac{8}{5} C^5 (1-2C)^2 [2 - y_R + 2C(y_R - 1)] \\ & \times \{2C[6 - 3y_R + 3C(5y_R - 8)] \\ & + 4C^3[13 - 11y_R + C(3y_R - 2) + 2C^2(1 + y_R)] \\ & + 3(1 - 2C^2)^2 [2 - y_R + 2C(y_R - 1)] \ln(1 - 2C)\}^{-1}, \end{aligned} \tag{11}$$

where $y_R \equiv y(R)$ is the value of the function $y(r)$ at the edge of the star. This function satisfies the equation

$$r \frac{dy(r)}{dr} + y(r)^2 + y(r) F(r) + r^2 Q(r) = 0, \tag{12}$$

where

$$\begin{aligned} F(r) &= \frac{r - 4\pi r^3 [\varepsilon(r) - p(r)]}{r - 2m(r)}, \\ Q(r) &= \frac{4\pi r [5\varepsilon(r) + 9p(r) + \frac{\varepsilon(r) + p(r)}{\partial p(r)/\partial \varepsilon(r)} - \frac{6}{4\pi r^2}]}{r - 2m(r)}. \end{aligned} \tag{13}$$

In (12) and (13), r is the radial variable measured from the centre of the star, $\varepsilon(r)$ and $p(r)$ are energy per baryon and pressure at r, and $m(r)$ is the mass inside the sphere of radius r. We use here the geometric unit system with $c = G = 1$. Starting at the centre of the star, for a given EOS, equation (12) is integrated self-consistently together with the Tolman–Oppenheimer–Volkoff equation, at various central densities with the boundary condition at the centre $y(0) = 2$, to obtain the $k_2(R)$ dependence. This together with expression (10) and the mass–radius dependence give us the dependences of tidal deformability Λ on mass M and radius R.

From the GW170817 event, the LIGO-Virgo collaboration has extracted [37,55,56]:

$$M_{chirp} = 1.186^{+0.001}_{-0.001} M\odot \tag{14}$$

$$\overline{\Lambda} = 300^{+420}_{-230}\,, \tag{15}$$

where M_{chirp} [57] and $\overline{\Lambda}$ [41,58] are averaged quantities determined by the individual $m_1, m_2, \Lambda_1, \Lambda_2$ of the two stars merged:

$$M_{chirp} = \frac{(m_1 m_2)^{3/5}}{(m_1 + m_2)^{1/5}} \tag{16}$$

$$\overline{\Lambda} = \frac{16}{13} \frac{(m_1 + 12m_2)m_1^4 \Lambda_1 + (m_2 + 12m_1)m_2^4 \Lambda_2}{(m_1 + m_2)^5} \tag{17}$$

If one of the stars has the "standard" mass $1.4M_\odot$, its deformability and radius satisfy the following constraints [37,55,56]:

$$\Lambda = 70 - 580 \tag{18}$$

$$R = 10.5 - 13.3 \text{ km}. \tag{19}$$

We use these constraints as well as the condition $M_{max} > 2M_\odot$ in the selection of the equation of state.

3. Results and Discussion

As a first step, we consider nucleon matter without hyperons and employ six parametrizations of the NN interaction: SLy230a [34], SLy4 [59], SkI3 [60], SkO [61], SkM* [62] and SkX [63].

The choice of Skyrme NN-forces relevant for studying neutron star matter has been considered earlier. It was shown in [33] that in the case of interactions SkM* and SkX, the proton fraction disappears at densities above $3n_0$ and the state of pure neutron matter becomes more energetically favourable. In [36], the density at the point of transition to the ferromagnetic state is used as a selection criterion, and the SkO parameter set is excluded by this criterion, although the equation of state in this case is in good agreement with other models [33]. Earlier in [64], we considered the correlations between the characteristics of nuclear matter equation of state and the neutron star properties on the example of 42 parametrizations of the Skyrme NN-force. The maximum mass of neutron star M_{max} and its corresponding radius R_{max} are most strongly related to the first and second derivatives of the symmetry energy with respect to density, which characterize the behaviour of the symmetry energy at high densities. Parameterization SkI3 leads to one of the highest values of M_{max} among the sets considered in [64].

Figure 1 shows the calculations of equation of state and dependencies of neutron star mass on the radius for the six listed parameters sets, including the results for the previously excluded SkX, SkM* and SkO. Parameterizations SkX and SkM* lead to overly soft equations of state and, as a result, the corresponding values of M_{max} do not reach 2 $M_\odot$ even without hyperons. For other parametrizations, the differences in the equations of state are not so significant and the $M(R)$ dependence turns out to be more sensitive to the properties of the interaction.

Figure 2 shows the dependencies of the tidal deformability Λ on the star radius and mass. Although the first experimental estimates of Λ make it possible to impose new restrictions on the model predictions (18) and (19), at this stage, these limits are quite wide and most of the interactions satisfy them or lay on the boundary.

For further considerations, we adopt the SkI3 and SLy230a parameter sets, which give the greatest maximum masses. Several predictions of bulk properties of nuclear matter made with parametrizations under consideration are summarized in Table 1.

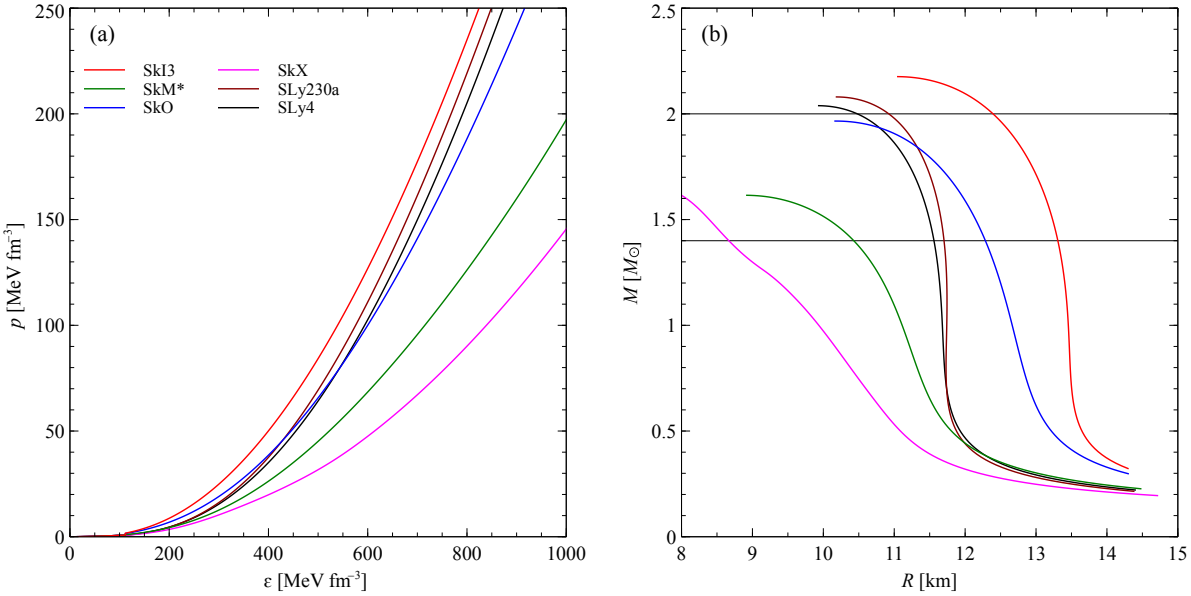

Figure 1. Neutron stars without hyperons with different parameterizations of NN interaction: (**a**) equation of state, (**b**) dependence of mass on radius.

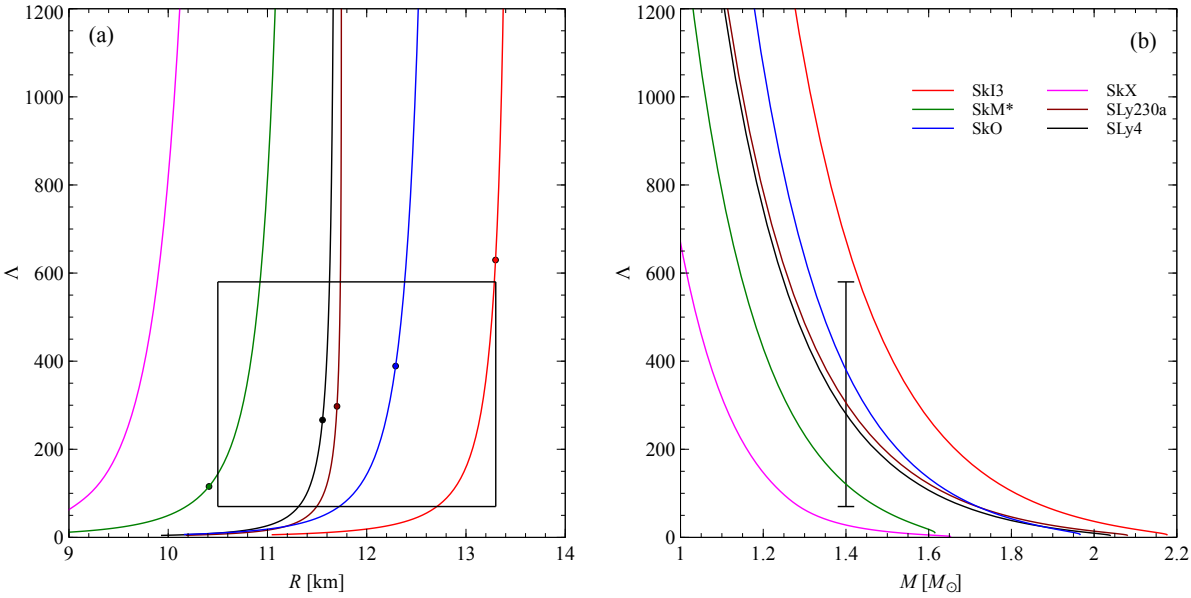

Figure 2. Dependence of tidal deformability for neutron star matter without hyperons for different parameterizations of NN interaction (**a**) on neutron star radius; (**b**) on neutron star mass. Dots in figure (**a**) correspond to neutron stars with $M = 1.4M_\odot$. The rectangle in (**a**) and interval in (**b**) represent restrictions (18) and (19).

Table 1. Symmetric nuclear matter saturation properties obtained with different NN-force Skyrme parametrizations (energy per particle at saturation E_0(MeV), incompressibility K_∞(MeV), the symmetry energy a_s(MeV) and its first and second derivatives at saturation L (MeV) and K_{sym}(MeV), effective mass $m^* = M^*/M$ (data are taken from [18]), and characteristics of neutron stars: maximum mass $M_{max}(M_\odot)$ and corresponding radius R_{max}(km).

Model	E_0	K_∞	a_s	L	K_{sym}	$m*$	M_{max}	R_{max}
SkI3	−15.98	258.19	34.83	100.53	73.04	0.58	2.19	10.93
SLy230a	−15.99	229.89	31.99	44.32	−98.22	0.70	2.08	10.18

Let us now include Λ hyperons. The parameters of ΛN interactions we use are presented in Table 2. Parameterizations YMR [65], LYI [66] and SLL4′ [67] provide the best description of the hypernuclear experimental data and can be considered realistic. Earlier parametrizations from [68] also describe the experiment satisfactorily. We use parameterizations YBZ2 with the largest three-body force and YBZ6 with especially strong non-locality.

Table 2. Parameters of employed ΛN interactions (u_0 is given in $MeVfm^3$, u_1 and u_2 in $MeVfm^5$, u_3 in $MeVfm^{3+3\gamma}$; other parameters are dimensionless).

Model	u_0	ξ_0	u_1	u_2	u_3	ξ_3	γ
YBZ2	−391.8	−0.085	56.95	48.05	3000	0	1
YBZ6	−372.2	−0.107	100.4	79.6	2000	0	1
SLL4′ *	−326	0	62	20	1880	0	1
YMR	−1056.2	0	96.248	8.743	2811.2	0	1/8
LYI	−476	−0.0452	42	23	1514.1	−0.280	1/3

* In [67], parameters u_0 and ξ_0 of the SLL4′ interaction are provided in the form of a single parameter $a_0 = u_0(1 + \xi_0/2)$.

The YBZ2 and YBZ6 sets were constructed with the three-body force (8), while the other sets involve the density-dependent force (9). For hypernuclei, the difference is insignificant. Below, we employ form (9), unless explicitly stated otherwise.

To describe the ΛΛ interaction, we use three sets of parameters, namely SΛΛ1′, SΛΛ2 and SΛΛ3′. The parameters of ΛΛ interactions we use are shown in Table 3.

Table 3. Parameters of employed ΛΛ interactions (λ_0 is given in $MeVfm^3$, λ_1 in $MeVfm^5$).

Model	λ_0	λ_1
SΛΛ1′	−37.9	14.1
SΛΛ2	−437.7	240.7
SΛΛ3′	−156.4	347.2

The SΛΛ1, SΛΛ2 and SΛΛ3 sets were obtained [45] using the fit to the data accepted at that time. These three sets effectively conform to a small, moderate and large interaction range, correspondingly. All the sets reproduce a strong ΛΛ attraction, as believed before the famous Nagara event [69].

When the ΛΛ attraction became much weaker, the SΛΛ1 and SΛΛ3 sets were modified accordingly and the SΛΛ1′ and SΛΛ3′ sets were obtained [70]. Note that SΛΛ2 set was not modified and the attraction remains strong in this case.

The equations of state with interaction SkI3 for nucleonic interaction and interactions SLL4′ and LYI for hyperon–nucleon interaction are depicted in Figure 3.

Figure 3 illustrates the "hyperon puzzle". It is seen that the equation of state becomes substantially softer when the hyperons are added. However, the softening with the LYI interaction is much larger than that obtained with the SLL4′ parameter set. The reason is that $\gamma = 1/3$ in the first case and $\gamma = 1$ in the second (for γ definition, see (9)). These two interactions give equally good descriptions of hypernuclear spectra [66,67], but the repulsion at high densities grows faster for $\gamma = 1$. Therefore, we can suggest that the neutron star studies require the ΛN interaction with $\gamma = 1$ or three-body ΛNN interactions. This point will be further discussed below.

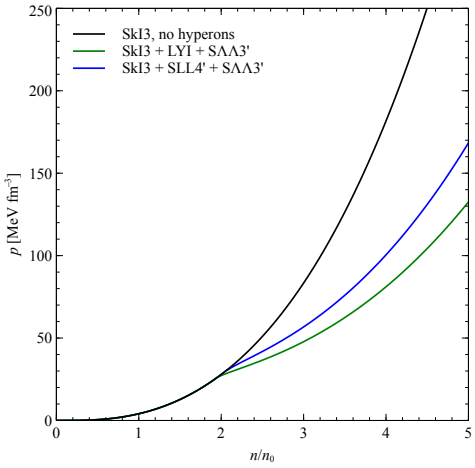

Figure 3. Equation of state without hyperons (black) and with hyperons for $\gamma = 1$ (SLL4′, blue) and $\gamma = 1/3$ (LYI, green). The nucleon interaction is SkI3 and the $\Lambda\Lambda$ interaction is S$\Lambda\Lambda$3′.

In Figure 4, fractions of nucleons, hyperons and leptons are presented as functions of the density. It is seen that the Λ fraction grows rapidly with density.

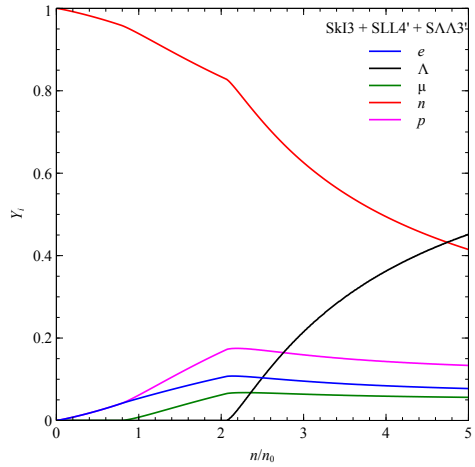

Figure 4. Dependence of fractions Y_i ($i = e, \Lambda, \mu, n, p$) of different particles on density for a certain combination of parameterizations of NN, ΛN and $\Lambda\Lambda$ forces.

One may naively suppose that Y_Λ never exceeds Y_p and Y_n since $m_\Lambda > m_N$. However, $Y_\Lambda > Y_n$ at high densities is a typical result, which is also encountered in other studies performed within other (not Skyrme) approaches. The reason is that repulsive forces become dominant at high densities. Repulsive forces are parameterized here via (8) and (9) (for comparison, $\Lambda\Lambda\omega$ coupling is used to describe repulsive forces in the relativistic mean field theory). All the ΛN forces compatible with hypernuclear spectra contain the many-body force (8) or (9), which is much weaker than (6) and (7) in nucleon interaction. Due to the stronger repulsive forces (6) and (7), the neutron chemical potential grows with density more rapidly than the hyperon chemical potential, and so the neutron fraction is depleted. Therefore, the system prefers more and more hyperons, which repel relatively weakly.

We stress that the softening of the equation of state, the "hyperon puzzle" and the hyperon excess at high densities have the same origin. The weaker the hyperonic repulsion (many-body effect in our approach) is, the more abundant hyperons are and the softer the equation of state is.

Figure 5 displays the $M(R)$ dependence. We compare three cases here: the non-interacting hyperons, hyperons interacting with nucleons, but not with each other, and the full set of interactions.

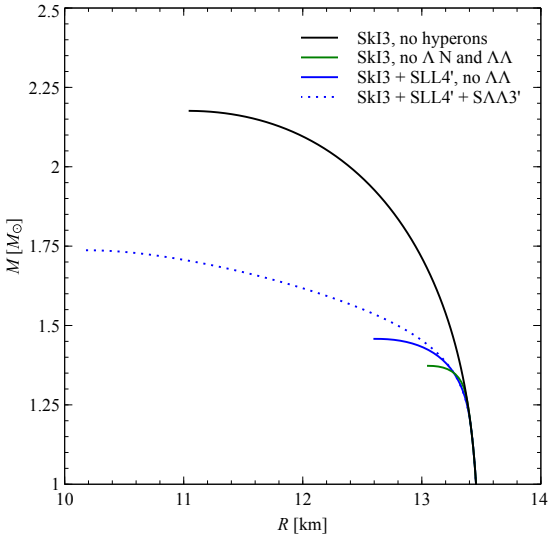

Figure 5. Dependence of neutron star mass on radius for different cases: without hyperons (black), with non-interacting hyperons (green), hyperons interacting with nucleons, but not with each other (solid blue), and with a full set of interactions (dotted blue).

It is interesting that non-interacting hyperons result in the smallest maximum mass and, therefore, the softest equation of state. At nuclear densities, the hyperon–nucleon interaction is presumably attractive, as known from hypernuclear studies. Switching off the ΛN interaction, we cancel not only this attraction, but also the short-range repulsion. It appears that the second point is more important for neutron stars, and the omission of ΛN interaction leads to a softer equation of state.

In Figure 6, we compare the density-dependent interactions with $\gamma = 1$ and the three-body ΛNN forces.

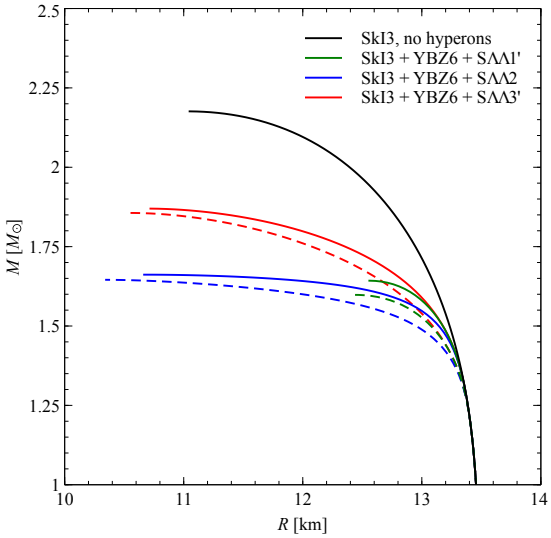

Figure 6. Dependence of neutron star mass on radius obtained with different parameterizations of $\Lambda\Lambda$ interaction. Dashed lines correspond to calculations with three-body forces; solid lines correspond to calculations with density-dependent forces.

We recall that (8) and (9) are equivalent in the symmetric matter at $\gamma = 1$ and $\xi_3 = 0$. The maximum mass for the density-dependent force is always larger than that for the three-body force. Skyrme three-body interactions (8) in the Λnn (and Λpp) system acts only on a singlet nn pair, while the density-dependent force does not discriminate between various spin states. Therefore, the repulsion in the first case weakens. However, the effect is not large, as seen from Figure 6.

In the same figure, we demonstrate the differences between the $M(R)$ dependencies for different $\Lambda\Lambda$ forces. It should be noted that the $\Lambda\Lambda$ interaction is known rather poorly and the S$\Lambda\Lambda$1′, S$\Lambda\Lambda$2 and S$\Lambda\Lambda$3′ sets are rather simplified since they contain neither the p-wave contribution nor any many-body effects. However, it may still be instructive to verify some interesting features even with these simplified potentials.

The short-range S$\Lambda\Lambda$1′ interaction does not affect the maximum mass strongly, but increases the corresponding (minimal) radius considerably. Since the $\Lambda\Lambda$ interaction becomes rather strong at high densities in this case, further contraction leads to instability. At the same time, the strong $\Lambda\Lambda$ attraction of the moderate range (the S$\Lambda\Lambda$2 set) leads to smaller minimal radii, but does not significantly change the maximum mass. The long-range S$\Lambda\Lambda$3′ set results in larger maximum masses. However, we recall that the $\Lambda\Lambda$ interaction employed here is incomplete and the results should be interpreted with caution.

In Figure 7, the $M(R)$ dependence for all the hyperonic interactions used is shown.

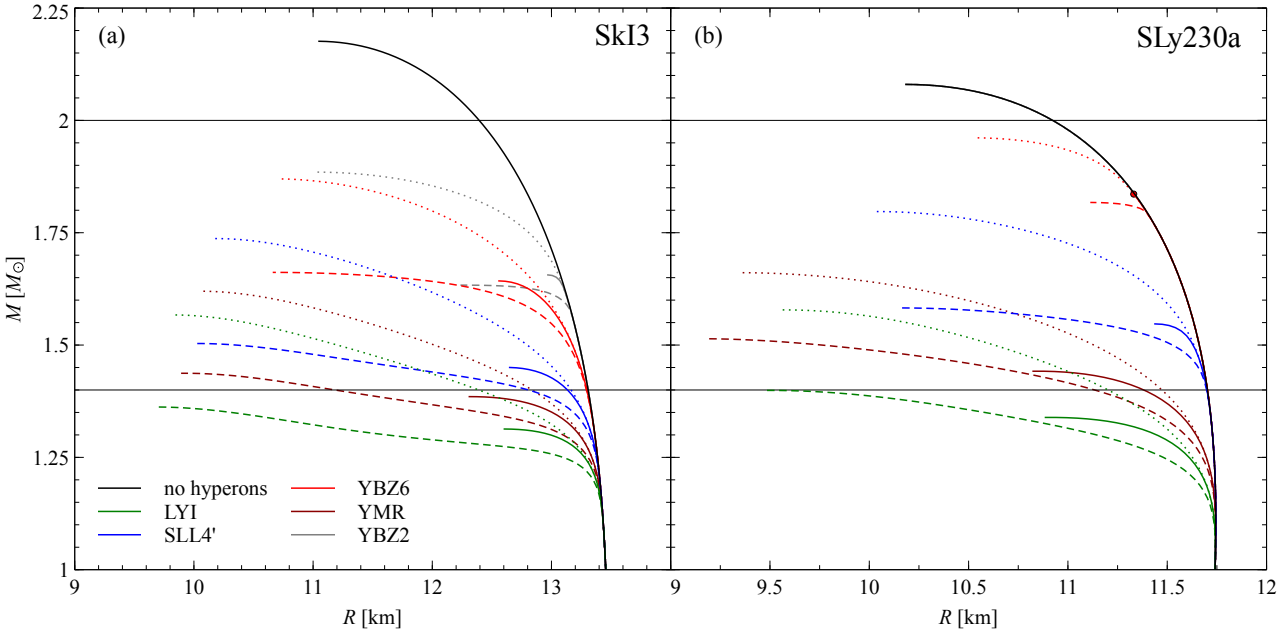

Figure 7. Dependence of neutron star mass on radius with different parameterizations of the ΛN and $\Lambda\Lambda$ forces and the SkI3 parameterization (**a**), the SLy230a (**b**) parameterization of the NN force. Different line types correspond to the different parameterizations of $\Lambda\Lambda$ interaction: S$\Lambda\Lambda$1′ (solid), S$\Lambda\Lambda$2 (dashed), S$\Lambda\Lambda$3′ (dotted). In Figure (**b**), the dot shows the maximum mass of a neutron star obtained with the combinations of parameter sets SLy230a + YBZ6 + S$\Lambda\Lambda$1′. In the SLy230a+YBZ2 case, hyperons do not appear so the curves for the YBZ2 set in panel (**b**) coincide with the curve for the pure nucleonic matter.

The interactions with $\gamma = 1$ evidently result in larger maximum masses, in accordance with the discussion above. We see once again that hyperons in the case of S$\Lambda\Lambda$1′ interaction extend to neutron stars, i.e., the radius corresponding to the maximum mass (the minimal radius) becomes larger.

No combination of interactions yields the maximum mass of $2M_{\odot}$. For the SkI3 interaction, the addition of hyperons lowers the maximum mass substantially. The YBZ2 set with a high-density-dependent term produces relatively better results.

On the other hand, lowering the maximum mass via hyperons is weaker for the SLy230a interaction. In this case, the hyperons appear at higher densities than in the SkI3 case, and in combination with YBZ2, hyperons do not appear at all. As a result, the equation of state is softened to a smaller degree.

To describe this situation in more detail, we introduce the binding energy of Λ-hyperon in the pure nucleonic matter:

$$D_{\Lambda} = -\mu_{\Lambda}. \tag{20}$$

From hypernuclear studies, D_{Λ} is known to be about 30 MeV at the normal nuclear density. At higher densities, D_{Λ} decreases and becomes negative due to the three-body or density-dependent forces.

We also introduce the critical energy of Λ-hyperons in the nucleonic matter:

$$D_{\Lambda}^{cr} = m_{\Lambda} - m_n - \mu_n. \tag{21}$$

Hyperons appear when the following condition is fulfilled: [71]

$$D_{\Lambda} = D_{\Lambda}^{cr}. \tag{22}$$

Note that D_{Λ} does not depend on the choice of the NN interaction if the density-dependent force (9) is employed (for the three-body force (8), the dependence is weak), and D_{Λ}^{cr} does not depend on the hyperonic interaction otherwise.

Figure 8 depicts the density dependence of D_{Λ} for different parameterizations of the ΛN interaction and D_{Λ}^{cr} for two parameterizations of the NN interaction (SkI3 and SLy230a) in nucleonic matter. The intersection point of D_{Λ} and D_{Λ}^{cr} corresponds to the point of appearance of hyperons.

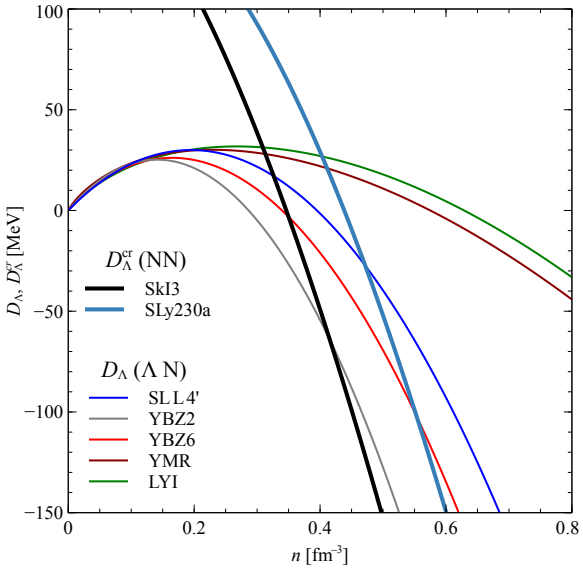

Figure 8. The density dependence of D_{Λ} for different parameterizations of the ΛN interaction and D_{Λ}^{cr} for two parameterizations of the NN interaction in nucleonic matter.

We see from Figure 8 that in the case of YBZ2 and SLy230a, D_{Λ} does not cross D_{Λ}^{cr} and hyperons do not appear. Note also that for each parameterization of the NN interaction, there is a clear correlation between the density of the appearance of hyperons and the maximum mass of a neutron star: a higher density corresponds to a higher maximum mass.

Seemingly, the simplest way to resolve the hyperon puzzle is to prove that hyperons cannot appear in neutron stars. It can be shown that large three-body or density-dependent forces can support such a conjecture, which was already noted in [13,15,17]. However, the majority of realistic hyperon–nucleon interactions employed here include the three-body or density-dependent forces not strong enough to prevent hyperon appearance, as seen from Figure 8. The single exception is the YBZ2 set when used together with SLy230a. Parameter set YBZ2, with the largest three-body force, should be considered "borderline realistic". The description of hypernuclear spectra with this set is acceptable, but somewhat worse [66] than with the other employed sets. Therefore, it seems unlikely, but not fully improbable, that the ΛN interactions compatible with hypernuclear data can exclude hyperons from neutron star matter. This straightforward solution is probably inappropriate.

As seen from Figure 7, the SLy230a + YBZ6 + S$\Lambda\Lambda 3^{'}$ combination results in a maximum mass rather close to $2M_{\odot}$. We cannot state that this combination should be treated as a "genuine" one, but we pinpoint the directions in which to search for suitable parameterizations.

In Figure 9, the tidal deformability as a function of radius is displayed.

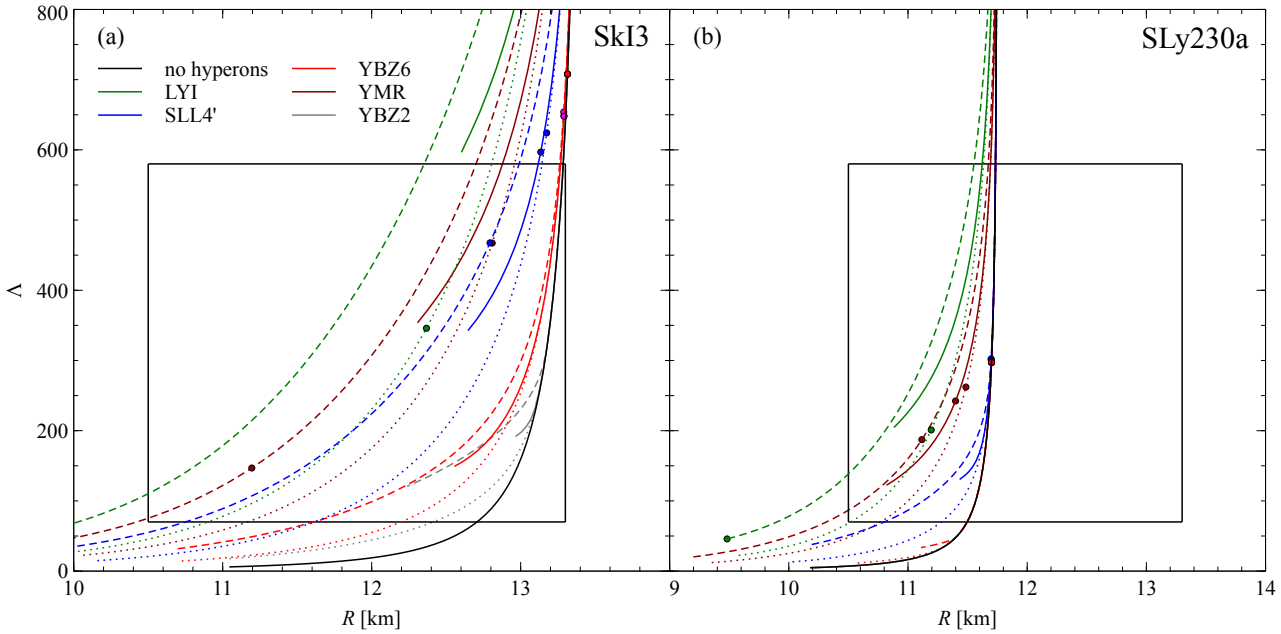

Figure 9. Tidal deformability dependence on neutron star radius with different parameterizations of the ΛN and $\Lambda\Lambda$ forces with the SkI3 parameterization (**a**), SLy230a parameterization (**b**) of the NN force. Different line types correspond to different parameterizations of the $\Lambda\Lambda$ interaction: S$\Lambda\Lambda 1'$ (solid), S$\Lambda\Lambda 2$ (dashed), S$\Lambda\Lambda 3'$ (dotted). The rectangles are the same as in Figure 2a. The dots correspond to $M = 1.4M_{\odot}$.

It is interesting that the combinations of interactions providing good results for the tidal deformability produce rather low maximum masses in the SkI3 case. At the same time, the combinations offering large maximum masses also provide acceptable tidal deformabilities in the SLy230a case.

Characteristics of neutron stars for all used interactions are also presented in Table 4. Note that for certain combinations of NN and ΛN interactions, namely SkI3+YBZ2 and SLy230a+YBZ6, hyperons appear at densities higher than those corresponding to $M = 1.4M_{\odot}$, which was already illustrated in Figure 7. For these combinations, Table 4 includes values of $R_{1.4}$ and $\Lambda_{1.4}$ corresponding to nucleonic matter. Moreover, for SLy230a+YBZ2, all values correspond to nucleonic matter, since hyperons do not appear in this case.

Table 4. Characteristics of neutron stars with different parameterizations of ΛN and $\Lambda\Lambda$ forces and SkI3 and SLy230a NN interactions. Table contains the following characteristics: radius of neutron star with $M = 1.4M_\odot$ ($R_{1.4}$, km) and corresponding tidal deformability $\Lambda_{1.4}$, maximum mass of the star M_{max}, ($M_\odot$), and corresponding radius R_{max}, km.

ΛN	$\Lambda\Lambda$	SkI3				SLy230a			
		$R_{1.4}$	$\Lambda_{1.4}$	M_{max}	R_{max}	$R_{1.4}$	$\Lambda_{1.4}$	M_{max}	R_{max}
LYI	S$\Lambda\Lambda$1′	-	-	1.31	12.6	-	-	1.34	10.9
	S$\Lambda\Lambda$2	-	-	1.36	9.7	9.5	46	1.40	9.5
	S$\Lambda\Lambda$3′	12.4	346	1.58	9.8	11.2	201	1.58	9.6
SLL4′	S$\Lambda\Lambda$1′	13.1	597	1.45	12.6	11.7	300	1.55	11.4
	S$\Lambda\Lambda$2	12.8	468	1.50	10.0	11.7	302	1.58	10.2
	S$\Lambda\Lambda$3′	13.1	624	1.74	10.2	11.7	301	1.80	10.0
YBZ6	S$\Lambda\Lambda$1′	13.3	648	1.64	12.6	11.7	297	1.84	11.3
	S$\Lambda\Lambda$2	13.3	654	1.66	10.7	11.7	297	1.82	11.1
	S$\Lambda\Lambda$3′	13.3	649	1.87	10.7	11.7	297	1.96	10.5
YBZ2 *	S$\Lambda\Lambda$1′	13.3	708	1.66	13.0	11.7	297	2.08	10.2
	S$\Lambda\Lambda$2	13.3	708	1.57	10.5	11.7	297	2.08	10.2
	S$\Lambda\Lambda$3′	13.3	708	1.83	10.7	11.7	297	2.08	10.2
YMR	S$\Lambda\Lambda$1′	-	-	1.39	12.3	11.4	242	1.44	10.8
	S$\Lambda\Lambda$2	11.2	147	1.44	9.9	11.1	187	1.51	9.2
	S$\Lambda\Lambda$3′	12.9	503	1.62	10.0	11.5	262	1.66	9.3

* In the SLy230a+YBZ2 case, Λ-hyperons do not appear, so the results for pure nucleonic matter are shown.

4. Conclusions

A very popular instrument in nuclear physics, the approach based on Skyrme interactions is not used as widely in neutron star studies, probably due to its non-relativistic nature. Naturally, relativistic mean field theory and similar approaches have advantages. However, the rich experience gathered in nuclear and hypernuclear theory with Skyrme interactions can also be rather helpful in the field of neutron stars. We note that superluminosity certainly does not manifest in full in our calculations. Here, we study the implications of various features of Skyrme interactions, mainly the ΛN one.

Density-dependent and three-body forces are a necessary part of Skyrme interactions. ΛNN or ΛN forces proportional to various powers of nuclear densities γ are usually treated as equally possible in hypernuclear physics. However, different γ′s lead to substantially different equations of state in neutron stars. Moreover, density-dependent forces even at $\gamma = 1$ become no longer equivalent to the ΛNN forces.

Properties of neutron star matter at high densities play a crucial role for maximum neutron star mass and resolution in the hyperon puzzle. Therefore, while various parameters of the Skyrme interaction are equally important at normal nuclear densities (in hypernuclei), the density-dependent or three-body forces dominate in neutron stars. They determine the point of hyperon appearance, hyperon abundance and the stiffness of the equation of state. We show that the best interactions from hypernuclear studies do not prevent hyperon appearance, so the hyperon puzzle still stands.

We used an oversimplified $\Lambda\Lambda$ interaction since the empirical information in this field is rather scarce. At large Λ abundances, this interaction may be too crude. Note that three-body zero-range $\Lambda\Lambda\Lambda$ force results in exactly zero due to the Pauli principle, but $\Lambda\Lambda N$ forces are possible. The $\Lambda\Lambda$ force, depending on the nucleon density, has been derived in [66] and already has been used in [72] for the equation of state of neutron star matter.

We restricted ourselves here with Λ hyperons since Λ hypernuclei are studied much better than the other ones. However, the Skyrme ΞN interaction has also been derived previously[73–75], so our consideration can be extended to a more realistic composition of neutron star matter.

Author Contributions: Conceptualization, D.L.; methodology, D.L. and T.T.; software, S.M. and A.N.; investigation, S.M. and A.N.; data curation, S.M. and A.N.; writing—original draft preparation, S.M. and A.N.; writing—review and editing, D.L. and T.T.; supervision, D.L. and T.T. All authors have read and agreed to the published version of the manuscript.

Funding: This research received no external funding.

Data Availability Statement: The data are available upon reasonable request.

Acknowledgments: Authors thank the Interdisciplinary Scientific and Educational School of Moscow University «Fundamental and Applied Space Research» for support. S.A. Mikheev expresses gratitude to the Theoretical Physics and Mathematics Advancement Foundation «BASIS». We would like to thank the organizers of the conference Infinite and Finite Nuclear Matter (INFINUM-2023), where the results of this paper were reported. We are also grateful to S.V. Sidorov for his help in editing the article.

Conflicts of Interest: The authors declare no conflict of interest.

References

1. Özel, F.; Freire, P. Masses, Radii, and the Equation of State of Neutron Stars. *Annu. Rev. Astron. Astrophys.* **2016**, *54*, 401–440. [CrossRef]
2. Lattimer, J.M. Neutron Star Mass and Radius Measurements. *Universe* **2019**, *5*, 159. [CrossRef]
3. Demorest, P.B.; Pennucci, T.; Ransom, S.M.; Roberts, M.S.E.; Hessels, J.W.T. A two-solar-mass neutron star measured using Shapiro delay. *Nature* **2010**, *467*, 1081–1083. [CrossRef] [PubMed]
4. Arzoumanian, Z.; Brazier, A.; Burke-Spolaor, S.; Chamberlin, S.; Chatterjee, S.; Christy, B.; Cordes, J.M.; Cornish, N.J.; Crawford, F.; Cromartie, H.T.; et al. The NANOGrav 11-year Data Set: High-precision Timing of 45 Millisecond Pulsars. *Astrophys. J. Suppl. Ser.* **2018**, *235*, 37. [CrossRef]
5. Antoniadis, J.; Freire, P.C.C.; Wex, N.; Tauris, T.M.; Lynch, R.S.; van Kerkwijk, M.H.; Kramer, M.; Bassa, C.; Dhillon, V.S.; Driebe, T.; et al. A Massive Pulsar in a Compact Relativistic Binary. *Science* **2013**, *340*, 1233232. [CrossRef]
6. Cromartie, H.T.; Fonseca, E.; Ransom, S.M.; Demorest, P.B.; Arzoumanian, Z.; Blumer, H.; Brook, P.R.; DeCesar, M.E.; Dolch, T.; Ellis, J.A.; et al. Relativistic Shapiro delay measurements of an extremely massive millisecond pulsar. *Nat. Astron.* **2019**, *4*, 72–76. [CrossRef]
7. Fonseca, E.; Cromartie, H.T.; Pennucci, T.T.; Ray, P.S.; Kirichenko, A. Y.; Ransom, S.M.; Demorest, P.B.; Stairs, I.H.; Arzoumanian, Z.; Guillemot, L.; et al. Refined Mass and Geometric Measurements of the High-mass PSR J0740+6620. *Astrophys. J. Lett.* **2021**, *915*, L12. [CrossRef]
8. Romani, R.W.; Kandel, D.; Filippenko, A.V.; Brink, T.G.; Zheng, W. PSR J0952–0607: The Fastest and Heaviest Known Galactic Neutron Star. *Astrophys. J. Lett.* **2022**, *934*, L17. [CrossRef]
9. Riley, T.E.; Watts, A.L.; Ray, P.S.; Bogdanov, S.; Guillot, S.; Morsink, S.M.; Bilous, A.V.; Arzoumanian, Z.; Choudhury, D.; Deneva, J.S.; et al. A NICER View of the Massive Pulsar PSR J0740+6620 Informed by Radio Timing and XMM-Newton Spectroscopy. *Astrophys. J. Lett.* **2021**, *918*, L27. [CrossRef]
10. Miller, M.C.; Lamb, F.K.; Dittmann, A.J.; Bogdanov, S.; Arzoumanian, Z.; Gendreau, K.C.; Guillot, S.; Ho, W.C.G.; Lattimer, J.M.; Loewenstein, M.; et al. The Radius of PSR J0740+6620 from NICER and XMM-Newton Data. *Astrophys. J. Lett.* **2021**, *918*, L28. [CrossRef]
11. Salmi, T.; Vinciguerra, S.; Choudhury, D.; Riley, T.E.; Watts, A.L.; Remillard, R.A.; Ray, P.S.; Bogdanov, S.; Guillot, S.; Arzoumanian, Z.; et al. The Radius of PSR J0740+6620 from NICER with NICER Background Estimates. *Astrophys. J.* **2022**, *941*, 150. [CrossRef]
12. Bombaci, I. The Hyperon Puzzle in Neutron Stars. *J. Phys. Soc. Jpn. Conf. Proc.* **2017**, *17*, 101002. [CrossRef]
13. Friedman, E.; Gal, A. Constraints from Λ hypernuclei on the ΛNN content of the Λ-nucleus potential. *Phys. Lett. B* **2023**, *837*, 137669. [CrossRef]
14. Vidaña, I. Neutron stars and the hyperon puzzle. *EPJ Web Conf.* **2022**, *271*, 09001. [CrossRef]
15. Takatsuka, T.; Nishizaki, S.; Yamamoto, Y. Necessity of extra repulsion in hypernuclear systems: Suggestion from neutron stars. *Eur. Phys. J. A* **2002**, *13*, 213–215. [CrossRef]
16. Lonardoni, D.; Lovato, A.; Gandolfi, S.; Pederiva, F. Hyperon Puzzle: Hints from Quantum Monte Carlo Calculations. *Phys. Rev. Lett.* **2015**, *114*, 092301. [CrossRef]
17. Gerstung, D.; Kaiser, N.; Weise, W. Hyperon–nucleon three-body forces and strangeness in neutron stars. *Eur. Phys. J. A* **2020**, *56*, 175. [CrossRef]
18. Dutra, M.; Lourenço, O.; Martins, S.; Delfino, A.; Stone, J.R.; Stevenson, P.D. Skyrme interaction and nuclear matter constraints. *Phys. Rev. C* **2012**, *85*, 035201. [CrossRef]
19. Del Popolo, A.; Deliyergiyev, M.; Le Delliou, M. Solution to the hyperon puzzle using dark matter. *Phys. Dark Universe* **2020**, *30*, 100622. [CrossRef]

20. Glendenning, N.K. Neutron stars are giant hypernuclei? *Astrophys. J.* **1985**, *293*, 470–493. [CrossRef]
21. Sedrakian, A.; Li, J.J.; Weber, F. Heavy baryons in compact stars. *Prog. Part. Nucl. Phys.* **2023**, *131*, 104041. [CrossRef]
22. Bednarek, I.; Manka, R. The role of nonlinear vector meson interactions in hyperon stars. *J. Phys. G Nucl. Part. Phys.* **2009**, *36*, 095201. [CrossRef]
23. Bednarek, I. Hyperon puzzle in compact stars. *Phys. Part. Nucl.* **2015**, *46*, 816–820. [CrossRef]
24. Oertel, M.; Providência, C.; Gulminelli, F.; Raduta, A. Hyperons in neutron star matter within relativistic mean-field models. *J. Phys. G Nucl. Part. Phys.* **2014**, *42*, 075202. [CrossRef]
25. Maslov, K.A.; Kolomeitsev, E.E.; Voskresensky, D.N. Making a soft relativistic mean-field equation of state stiffer at high density. *Phys. Rev. C* **2015**, *92*, 052801. [CrossRef]
26. Weissenborn, S.; Chatterjee, D.; Schaffner-Bielich, J. Hyperons and massive neutron stars: Vector repulsion and SU(3) symmetry. *Phys. Rev. C* **2012**, *85*, 065802. [CrossRef]
27. van Dalen, E.N.E.; Colucci, G.; Sedrakian, A. Constraining hypernuclear density functional with Λ-hypernuclei and compact stars. *Phys. Lett. B* **2014**, *734*, 383–387. [CrossRef]
28. Fortin, M.; Avancini, S.S.; Providência, C.; Vidaña, I. Hypernuclei and massive neutron stars. *Phys. Rev. C* **2017**, *95*, 065803. [CrossRef]
29. Li, J.J.; Long, W.H.; Sedrakian, A. Hypernuclear stars from relativistic Hartree-Fock density functional theory. *Eur. Phys. J. A* **2018**, *54*, 133. [CrossRef]
30. Lim, Y.; Lee, C.-H.; Oh, Y. Effective interactions of hyperons and mass-radius relation of neutron stars. *Phys. Rev. D* **2018**, *97*, 023010. [CrossRef]
31. Li, Z.; Ren, Z.; Hong, B.; Lu, H.; Bai, D. Neutron stars within a relativistic mean field theory compatible with nucleon-nucleon short-range correlations. *Nucl. Phys. A* **2019**, *990*, 118–136. [CrossRef]
32. Fu, H.R.; Li, J.J.; Sedrakian, A.; Weber, F. Massive relativistic compact stars from SU(3) symmetric quark models. *Phys. Lett. B* **2022**, *834*, 137470. [CrossRef]
33. Rikovska Stone, J.; Miller, J.C.; Koncewicz, R.; Stevenson, P.D.; Strayer, M.R. Nuclear matter and neutron-star properties calculated with the Skyrme interaction. *Phys. Rev. C* **2003**, *68*, 034324. [CrossRef]
34. Chabanat, E.; Bonche, P.; Haensel, P.; Meyer, J.; Schaeffer, R. A Skyrme parametrization from subnuclear to neutron star densities. *Nucl. Phys. A* **1997**, *627*, 710–746. [CrossRef]
35. Lim, Y.; Hyun, C.H.; Kwak, K.; Lee, C.-H. Hyperon puzzle of neutron stars with Skyrme force models. *Int. J. Mod. Phys. E* **2015**, *24*, 1550100. [CrossRef]
36. Mornas, L. Neutron stars in a Skyrme model with hyperons. *Eur. Phys. J. A* **2005**, *24*, 293–312. [CrossRef]
37. Abbott, B.P.; Abbott, R.; Abbott, T.D.; Acernese, F.; Ackley, K.; Adams, C.; Adams, T.; Addesso, P.; Adhikari, R.X.; Adya, V.B.; et al. GW170817: Observation of Gravitational Waves from a Binary Neutron Star Inspiral. *Phys. Rev. Lett.* **2017**, *119*, 161101. [CrossRef]
38. Watson, D.; Hansen, C.J.; Selsing, J.; Koch, A.; Malesani, D.B.; Andersen, A.C.; Fynbo, J.P.U.; Arcones, A.; Bauswein, A.; Covino, S.; et al. Identification of strontium in the merger of two neutron stars. *Nature* **2019**, *574*, 497–500. [CrossRef]
39. Abbott, B.P.; Abbott, R.; Abbott, T.D.; Abraham, S.; Acernese, F.; Ackley, K.; Adams, C.; Adhikari, R.X.; Adya, V.B.; Affeldt, C.; et al. GW190425: Observation of a Compact Binary Coalescence with Total Mass $\sim 3.4\ M_{\odot}$. *Astrophys. J. Lett.* **2020**, *892*, L3. [CrossRef]
40. Thorne, K.S. Tidal stabilization of rigidly rotating, fully relativistic neutron stars. *Phys. Rev. D* **1998**, *58*, 124031. [CrossRef]
41. Flanagan, É. É.; Hinderer, T. Constraining neutron-star tidal Love numbers with gravitational-wave detectors. *Phys. Rev. D* **2008**, *77*, 021502. [CrossRef]
42. Vautherin, D.; Brink, D.M. Hartree-Fock Calculations with Skyrme's Interaction. I. Spherical Nuclei. *Phys. Rev. C* **1972**, *5*, 626–647. [CrossRef]
43. Rayet, M. Skyrme parametrization of an effective Λ-nucleon interaction. *Nucl. Phys. A* **1981**, *367*, 381–397. [CrossRef]
44. Hiyama, E.; Nakazawa, K. Structure of S = −2 Hypernuclei and hyperon-hyperon interactions. *Annu. Rev. Nucl. Part. Sci.* **2018**, *68*, 131–159. [CrossRef]
45. Lanskoy, D.E. Double-Λ hypernuclei in the Skyrme-Hartree-Fock approach and nuclear core polarization. *Phys. Rev. C* **1998**, *58*, 3351–3358. [CrossRef]
46. Millener, D.J.; Dover, C.B.; Gal, A. Λ-nucleus single-particle potentials. *Phys. Rev. C* **1988**, *38*, 2700–2708. [CrossRef]
47. Lanskoi, D.E.; Tret'yakova, T.Y. Skyrme interactions in calculations of hypernuclei by the Hartree–Fock method. *Sov. J. Nucl. Phys. (Engl. Transl.)* **1989**, *49*, 987–991.
48. Tolman, R.C. Static Solutions of Einstein's Field Equations for Spheres of Fluid. *Phys. Rev.* **1939**, *55*, 364–373. [CrossRef]
49. Oppenheimer, J.R.; Volkoff, G.M. On Massive Neutron Cores. *Phys. Rev.* **1939**, *55*, 374–381. [CrossRef]
50. Baym, G.; Pethick, C.; Sutherland, P. The Ground State of Matter at High Densities: Equation of State and Stellar Models. *Astrophys. J.* **1971**, *170*, 299. [CrossRef]
51. Baiotti, L. Gravitational waves from neutron star mergers and their relation to the nuclear equation of state. *Prog. Part. Nucl. Phys.* **2019**, *109*, 103714. [CrossRef]
52. Hinderer, T. Tidal Love Numbers of Neutron Stars. *Astrophys. J.* **2008**, *677*, 1216. [CrossRef]
53. Krastev, P.G.; Li, B.-A. Imprints of the nuclear symmetry energy on the tidal deformability of neutron stars. *J. Phys. Nucl. Part. Phys.* **2019**, *46*, 074001. [CrossRef]

54. Malik, T.; Alam, N.; Fortin, M.; Providência, C.; Agrawal, B.K.; Jha, T.K.; Kumar, B.; Patra, S.K. GW170817: Constraining the nuclear matter equation of state from the neutron star tidal deformability. *Phys. Rev. C* **2018**, *98*, 035804. [CrossRef]
55. Abbott, B.P.; Abbott, R.; Abbott, T.D.; Acernese, F.; Ackley, K.; Adams, C.; Adams, T.; Addesso, P.; Adhikari, R.X.; Adya, V.B.; et al. GW170817: Measurements of Neutron Star Radii and Equation of State. *Phys. Rev. Lett.* **2018**, *121*, 161101. [CrossRef]
56. Abbott, B.P.; Abbott, R.; Abbott, T.D.; Acernese, F.; Ackley, K.; Adams, C.; Adams, T.; Addesso, P.; Adhikari, R.X.; Adya, V.B.; et al. Properties of the Binary Neutron Star Merger GW170817. *Phys. Rev. X* **2019**, *9*, 011001. [CrossRef]
57. Cutler, C.; Flanagan, É.É. Gravitational waves from merging compact binaries: How accurately can one extract the binary's parameters from the inspiral waveform? *Phys. Rev. D* **1994**, *49*, 2658–2697. [CrossRef]
58. Favata, M. Systematic Parameter Errors in Inspiraling Neutron Star Binaries. *Phys. Rev. Lett.* **2014**, *112*, 101101. [CrossRef] [PubMed]
59. Chabanat, E.; Bonche, P.; Haensel, P.; Meyer, J.; Schaeffer, R. A Skyrme parametrization from subnuclear to neutron star densities. Part II. Nuclei far from stablities. *Nucl. Phys. A* **1998**, *635*, 231–256, Erratum: *Nucl. Phys. A* **1998**, *643*, 441–441. [CrossRef]
60. Reinhard, P.-G.; Flocard, H. Nuclear effective forces and isotope shifts. *Nucl. Phys. A* **1995**, *584*, 467–488. [CrossRef]
61. Reinhard, P.-G.; Dean, D.J.; Nazarewicz, W.; Dobaczewski, J.; Maruhn, J.A.; Strayer, M.R. Shape coexistence and the effective nucleon-nucleon interaction. *Phys. Rev. C* **1999**, *60*, 014316. [CrossRef]
62. Bartel, J.; Quentin, P.; Brack, M.; Guet, C.; Håkansson, H.-B. Towards a better parametrisation of Skyrme-like effective forces: A critical study of the SkM force. *Nucl. Phys. A* **1982**, *386*, 79–100. [CrossRef]
63. Brown, B.A. New Skyrme interaction for normal and exotic nuclei. *Phys. Rev. C* **1998**, *58*, 220–231. [CrossRef]
64. Mikheev, S.A.; Lanskoy, D.E.; Tretyakova, T.Y. Correlations between Properties of Nuclear Matter and Characteristics of Neutron Stars. *Phys. Part. Nucl.* **2022**, *53*, 409–414. [CrossRef]
65. Yamamoto, Y.; Motoba, T.; Rijken, T.A. G-Matrix Approach to Hyperon-Nucleus Systems. *Prog. Theor. Phys. Suppl.* **2010**, *185*, 72–105. [CrossRef]
66. Lanskoy, D.E.; Yamamoto, Y. Skyrme-Hartree-Fock treatment of Λ and ΛΛ hypernuclei with G-matrix motivated interactions. *Phys. Rev. C* **1997**, *55*, 2330–2339. [CrossRef]
67. Schulze, H.-J.; Hiyama, E. Skyrme force for light and heavy hypernuclei. *Phys. Rev. C* **2014**, *90*, 047301. [CrossRef]
68. Yamamoto, Y.; Bandō, H.; Žofka, J. On the Λ-Hypernuclear Single Particle Energies. *Prog. Theor. Phys.* **1988**, *80*, 757–761. [CrossRef]
69. Takahashi, H.; Ahn, J.K.; Akikawa, H.; Aoki, S.; Arai, K.; Bahk, S.Y.; Baik, K.M.; Bassalleck, B.; Chung, J.H.; Chung, M.S.; et al. Observation of a ${}^{6}_{\Lambda\Lambda}He$ Double Hypernucleus. *Phys. Rev. Lett.* **2001**, *87*, 212502. [CrossRef]
70. Minato, F.; Chiba, S. Fission barrier of actinide nuclei with double-Λ particles within the Skyrme–Hartree–Fock method. *Nucl. Phys. A* **2011**, *856*, 55–67. [CrossRef]
71. Imasheva, L.T.; Lanskoy, D.E.; Tretyakova, T.Y. Neutron Star Matter and Baryonic Interactions. *Phys. At. Nucl.* **2019**, *82*, 402–407. [CrossRef]
72. Balberg, S.; Barnea, N. S-wave pairing of Λ hyperons in dense matter. *Phys. Rev. C* **1998**, *57*, 409–416. [CrossRef]
73. Sun, T.T.; Hiyama, E.; Sagawa, H.; Schulze, H.-J.; Meng, J. Mean-field approaches for Ξ^- hypernuclei and current experimental data. *Phys. Rev. C* **2016**, *94*, 064319. [CrossRef]
74. Jin, Y.; Zhou, X.-R.; Cheng, Y.-Y.; Schulze, H.-J. Study of Ξ^- hypernuclei in the Skyrme-Hartree-Fock approach. *Eur. Phys. J. A* **2020**, *56*, 135. [CrossRef]
75. Guo, J.; Zhou, X.-R.; Schulze, H.-J. Skyrme force for all known Ξ^- hypernuclei. *Phys. Rev. C* **2021**, *104*, L061307. [CrossRef]

Disclaimer/Publisher's Note: The statements, opinions and data contained in all publications are solely those of the individual author(s) and contributor(s) and not of MDPI and/or the editor(s). MDPI and/or the editor(s) disclaim responsibility for any injury to people or property resulting from any ideas, methods, instructions or products referred to in the content.